Int. J. Electrochem. Sci., 12 **(2017)** 6853 – 6862, doi: 10.20964/2017.07.56

International Journal of
ELECTROCHEMICAL
SCIENCE
www.electrochemsci.org

Spinel $LiMn_2O_4$ with Two-step Nano-Al_2O_3 Coating as High Performance Positive Materials

Yannan Zhang[1], Peng Dong[2], Xiaohua Yu[3], Shubiao Xia[4], Jinjie Song[5], Ruiming Yang[1], Huixin Liang[2], Zhezhong Shi[1], Yao Yao[2], Xue Li[2,], Yingjie Zhang[1,*]*

[1] National and Local Joint Engineering Laboratory for Lithium-ion Batteries and Materials Preparation Technology, Key Laboratory of Advanced Battery Materials of Yunnan Province, Faculty of Materials Science and Engineering, Kunming University of Science and Technology, Kunming 650093, China.
[2] National and Local Joint Engineering Laboratory for Lithium-ion Batteries and Materials Preparation Technology, Key Laboratory of Advanced Battery Materials of Yunnan Province, Faculty of Metallurgical and Energy Engineering, Kunming University of Science and Technology, Kunming 650093, China
[3] National Engineering Research Center of Waste Resource Recovery, Kunming University of Science and Technology, Kunming 650093, China
[4] Faculty of Chemistry & Chemical Engineering, Qujing Normal University, Qujing 655011, China
[5] Key Laboratory of Mesoscale Severe Weather/Ministry of Education, and School of Atmospheric Sciences, Nanjing University, Nanjing 210093, China
[*]E-mail: 438616074@qq.com, zyjkmust@126.com

Received: 8 April 2017 / *Accepted:* 12 May 2017 / *Published:* 12 June 2017

To study the influence of the uniformity and integrity of amphoteric metal oxide coating layers on the performance of positive materials in Lithium-ion batteries, nano-Al_2O_3-coated $LiMn_2O_4$ positive material were synthesized by using a two-step sol-gel process. The products were characterized by power X-ray diffraction (XRD), scanning electron microscopy (SEM), Transmission Electron Microscopy (TEM), energy-dispersive X-ray spectrum (EDX), X-ray photoelectron spectroscopy (*XPS)*, galvanostatic charge-discharge test system, and inductively-coupled plasma emission spectrograph (ICP-AES). The results show that the two step method coating can bring with the uniform and glabrous nano-Al_2O_3 layer tightly coupling with the surface of the $LiMn_2O_4$ particles, when being positive material for Lithium-ion batteries, which exhibits capcity losses of only 13.2 % at 60 °C, after 300 cycles, much better than those of the pristine material and the sample synthesized by conventional one step sol-gel method (with the same Al_2O_3-coating content). Moreover, the ICP-AES tests of Mn^{2+} reveal that the Al_2O_3 layers with two step coating layer plays an important role in protecting $LiMn_2O_4$ from the electrolyte corrosion.

Keywords: $LiMn_2O_4$, sol-gel process, positive materials, lithium-ion batteries

1. INTRODUCTION

Lithium secondary batteries (LIB) have succeeded in various portable electronics, and considerable efforts have focused on developing a large-scale lithium-ion battery for use in electric vehicles (EVs), hybrid electric vehicles (HEVs) and energy storage systems (ESSs) [1-3]. $LiMn_2O_4$ is considered one of the most promising positive materials large-formate LIB applications due to its environmentally friendliness, high safety, richness in natural sources, and nontoxicity [4-6]. However , $LiMn_2O_4$-based batteries exhibit deteriorative capacity fading and poor rate capability during cycling or storage in the organic electrolytes at elevated temperatures. The fast capacity fading is mainly caused by dissolution of manganese into organic electrolyte, Jahn-Teller distortion and decomposition of electrolyte solution on the electrode[7-10].

The surface coating with metal oxides is considered to be a necessity to improve its performance[11-13], among various targeted materials proposed, amphoteric metal oxide coating is an effective route to enhance cycle ability and alter the surface chemistry for many electrode materials[14, 15], such as ZnO [16], Al_2O_3 [17], CaO [18], ZrO_2 [19], MgO [20], SiO_2 [21],GeO_2 [22], and La_2O_3 [23], has been widely undertaken. For most transition-metal-oxide based electrode like $LiMn_2O_4$, however, the uniformity and integrality of the coating substances is essential to decrease the Mn dissolution, the coating layer will be test severely, especially after the long cycling in the organic electrolytes at elevated temperatures [24].

In this paper, we have found a direct two-step coating route for improving $LiMn_2O_4$, the prepared product is named as $LiMn_2O_4$/ Al_2O_3-T. The influence of the two-step Al_2O_3 coating process on the crystal structure, particle morphology, electrochemical performances and the Mn^{2+} dissolution have been investigated in detail. Interestingly, compared with the pristine $LiMn_2O_4$ and the one-step coating sample(with the same coating amount), the surface morphology, electrochemical performances as well as the Mn^{2+} dissolution of the $LiMn_2O_4$/Al_2O_3-T have been found significantly improved.

2. EXPERIMENTAL

2.1 Sample preparation

$LiMn_2O_4$ was synthesized by the solid-state method. Electrolytic manganese dioxide (EMD) and 5 % mol excess lithium carbonate were mixed by ball grinding. The mixture was ignited in vacuum dryer followed by calcinations at 900 °C for 16 h to form the spinel $LiMn_2O_4$ powder. The Al_2O_3 coating modification is carried out by a sol-gel process. Stoichiometric aluminum nitrate and ammonium hydroxide were dissolved in ethanol solution with constant stirring to obtain the aluminous solution, then the $LiMn_2O_4$ powers were slowly added into the solution with vigorous agitation for 2 h at 80 °C. The pH value of the mixed solution was maintained at 8.0 by adding diluted ammonium hydroxide (20%). The resultant slurry was dried at 120 °C and subsequently sintered in air at 550 °C for 4 h to obtain the one-step coating sample (LMO/Al_2O_3). The prepared samples contain different contents of Al_2O_3 and the expected weight ratios of Al_2O_3 to $LiMn_2O_4$ are 0.75 wt% and 1.5 wt% respectively. After the natural cooling to room temperature, as prepared 0.75 wt%-LMO/Al_2O_3

powders were added into the same concentration and the volume aluminum of sol solution, subsequent mixing and drying process were similar with the previous procedures. Finally, the grounded powders were calcined in air at 550 °C for 4 h to obtain the two-step coating sample (1.5 wt%-LMO/Al_2O_3-T). The schematic diagram of the coating process is demonstrated in Figure 1. The pristine, one-step coating and two step coating samples were cited as $LiMn_2O_4$, $LiMn_2O_4$ /Al_2O_3 and $LiMn_2O_4$ /Al_2O_3-T respectively.

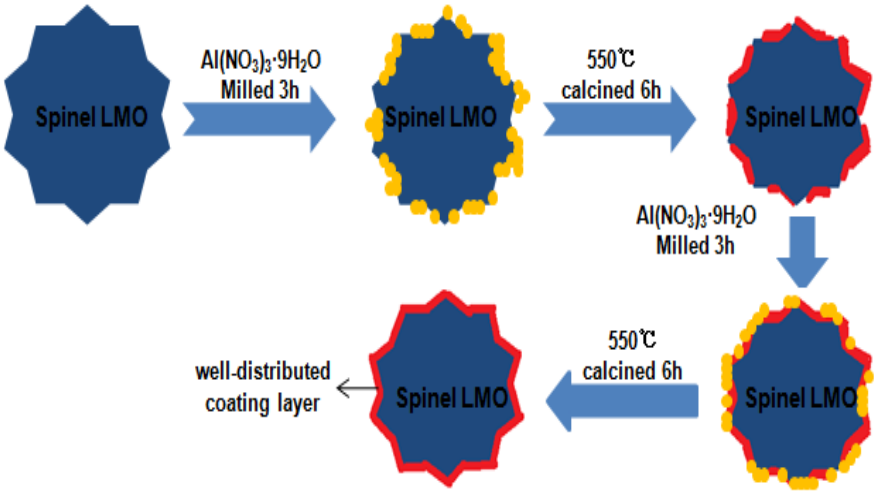

Figure 1. Schematic diagram of the two step coating process.

2.2 Characterization

The X-ray powder diffraction (XRD) measurements were performed on a diffractometer (Cu-K-α radiation , 40 kV, Rigaku, Rint-2000, Japan) in the 2θ range of 15 - 80°. Scanning electron microscope (SEM, TESCAN, 20 kV, Czech Republic) and transmittance electron microscopy (TEM, JEOL JEM-2010, Japan) were employed to measure the morphology and elemental mapping. The manganese ion dissolution and the ratios of coating elements from the active material were evaluated by inductively coupled plasma emission (ICP, Thermo-6000 America).

2.3 Electrochemical measurements

The electrochemical performances were performed using a standard CR2025 coin cell. The electrodes were prepared by casting and pressing a mixture of 80 wt.% $LiMn_2O_4$, 10 wt.% PVDF, and 10 wt.% carbon blacks in N-methyl pyrolidinone (NMP) onto aluminum foil and then drying for 12 h at 80 °C. Coin cells were fabricated in an argon-filled glove box, lithium metal foil was used as anode. and a solution of 1mol L^{-1} $LiPF_6$ electrolyte with EC: DEC: DMC = 1:1:1 (volume ratios) was used as electrode. The cells were charged and discharged on a battery tester (LAND CT-2010A, China) in the range of 3.0 - 4.5V (vs. Li/Li^+) with a current density of 0.24 mA g^{-1} -12 mA g^{-1} (0.2 C-10 C) at 60 °C.

3. RESULTS AND DISCUSSION

3.1. Structural and morphological characterization

The XRD patterns of the pristine, 1.5 wt%-LMO/Al_2O_3, and 1.5 wt%-LMO/Al_2O_3-T samples are shown in Fig. 1. All the diffraction peaks can be assigned to a well-defined spinel structure of $LiMn_2O_4$ with the space group *Fd3m*(JCPDS 88-1749), indicating that the bulk structure of the $LiMn_2O_4$ has no significant change after surface modification. No obvious diffraction peaks of Al_2O_3 are detected in the modified samples, which is likely due to the low weight ratio of 1.5 wt%. These results are in good agreement with the reports in the literature [26-28]. The lattice constants are calculated by Jade 6.0, both the pristine and surface-modified samples exhibit almost similar lattice parameters, suggesting that Al_2O_3 may be coated on the surface of the $LiMn_2O_4$ particles and no Al^{3+} enters into the bulk structure of spinel during the coating and sintering process.

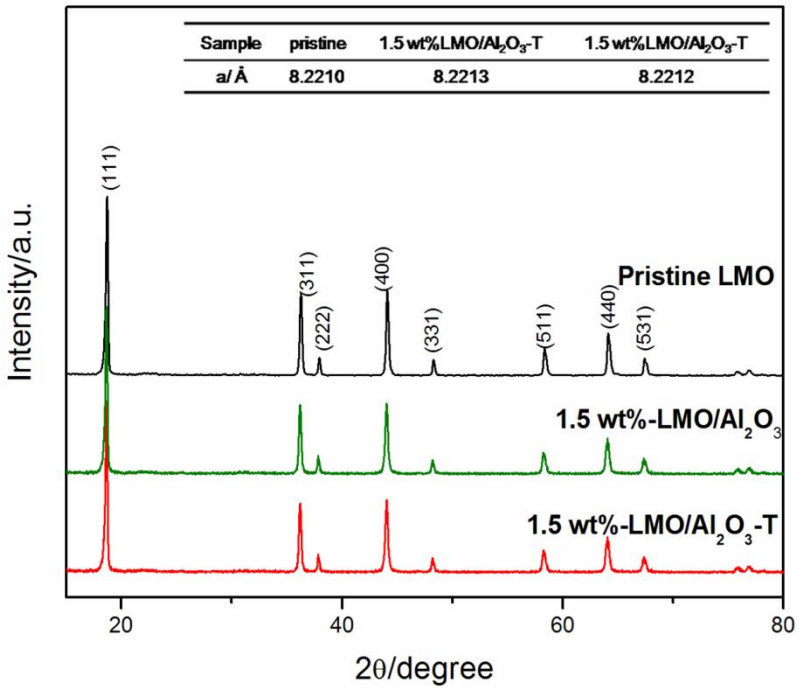

Figure 2. XRD patterns and lattice constants of the pristine $LiMn_2O_4$,$LiMn_2O_4/Al_2O_3$ and $LiMn_2O_4/Al_2O_3$-T. samples

SEM images and EDX pattern in Figure. 3 show the surface morphology information on pristine $LiMn_2O_4$, $LiMn_2O_4/Al_2O_3$ and $LiMn_2O_4/Al_2O_3$-T samples. As can be seen from Fig. 3(a), the pristine $LiMn_2O_4$ sample is highly crystallized with diameters less than 30 μm. Fig. 3(b) and (c) show that the surface of the powders changed noticeably upon coating. It is worthwhile mentioning that the coating layers are more smooth and compact after two-step modification (Figure. 3 (c)). The EDX pattern of the sample LMO/Al_2O_3-T is presented in Fig. 3(d), From Figure. 3 (d), it is found that Mn, O, and Al elements are detected in the EDX pattern, Al element is well distributed on the surface scanning area, which may indicate that the Al_2O_3 layers are formed successfully on the surface of the pristine $LiMn_2O_4$. This conclusion is to be expected and will be further discussed as below.

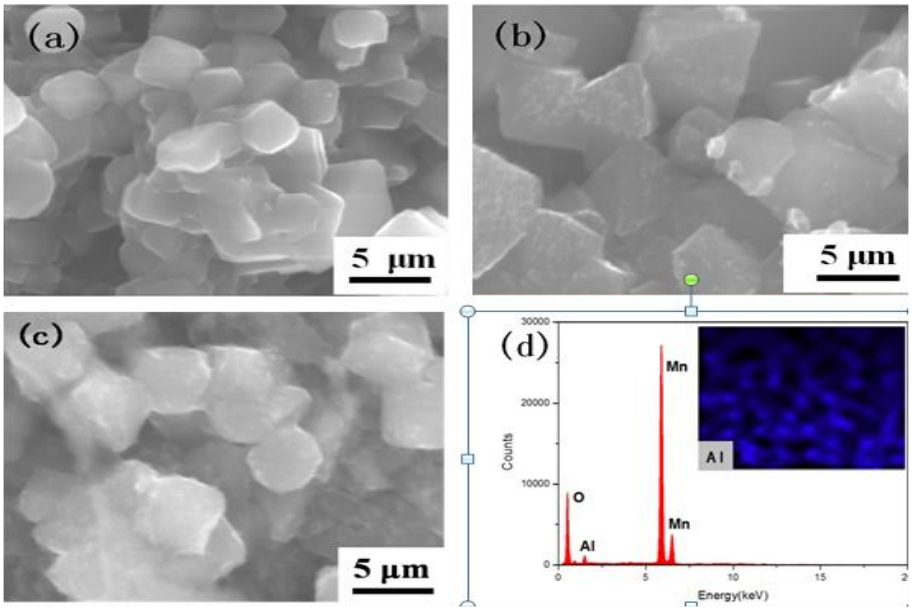

Figure 3. (a) SEM image of pristine $LiMn_2O_4$, (b) SEM image of $LiMn_2O_4$ /Al_2O_3, (c) SEM image of $LiMn_2O_4$ /Al_2O_3-T and (d) EDX map of the $LiMn_2O_4$ /Al_2O_3-T particles.

Figure. 4 compares the TEM images of the uncoated and two-step coated samples. The pristine $LiMn_2O_4$ sample (Figure. 4 (a)) shows well-crystallized particles clear grain boundary. As illustrated in Figure. 4 (b), Al_2O_3 coated sample shows an amorphous layer on the surface of $LiMn_2O_4$ core, Figure. 4 (c) is the partial enlarged image of (b), it is clear that there existed a distinguishable and translucent compact coating layer with the average thickness of about 20 nm on the surface of the $LiMn_2O_4$ particles in Figure. 4 (c). The Al_2O_3 on the surface of $LiMn_2O_4$ can also be confirmed from the selected-area electron diffraction (SAED) pattern as shown in Figure. 4 (c), the spots are indexed with the (111) and (002) planes of the Al_2O_3 phase (JCPDS#88-0107), this is consistent well with the observation from SEM–EDS in Figure. 3 as above [29].

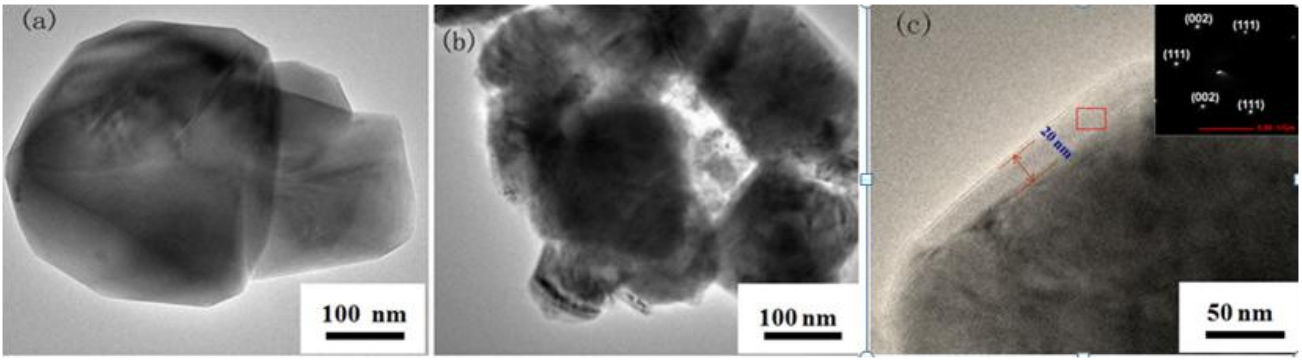

Figure 4. TEM images of pristine (a), $LiMn_2O_4$ /Al_2O_3-T (b) and the partial enlarged image of $LiMn_2O_4$ /Al_2O_3-T (c). 5.00 1/Gm

3.2. Electrochemical performance

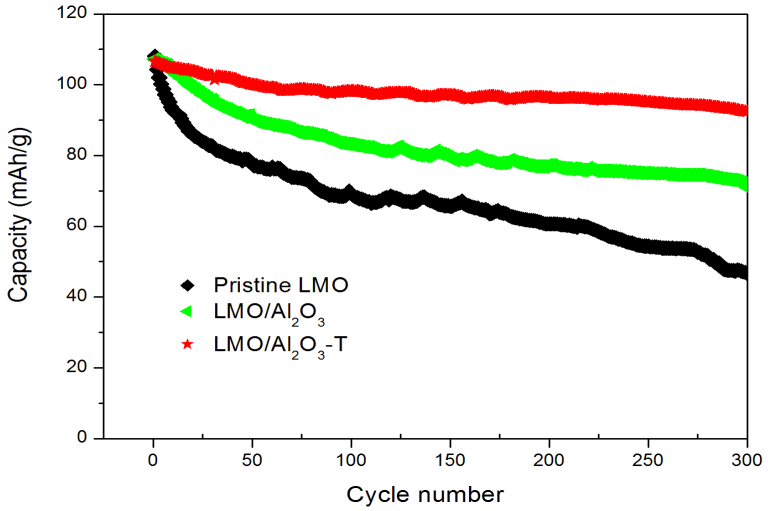

Figure 5. Cycling performance of the uncoated $LiMn_2O_4$, $LiMn_2O_4$ /Al_2O_3 and $LiMn_2O_4$/Al_2O_3-T at 60 °C and a 1 C charge/discharge rate

Table 1. Recently reported LIBs systems based on different materials modification of $LiMn_2O_4$.

Coating materials of $LiMn_2O_4$	Capcity retention and discharge capacity (mAh g^{-1}) after several cycles at certain rate and temperature
1 wt% MnO [30]	88.8%, 95.5, 100 cycles, 1C, 25 °C
2 wt% AlF_3 [31]	89.8%, 92.9, 100 cycles, 1C, 25 °C
10 wt% $LiNi_{0.5}Mn_{1.5}O_4$ [32]	81.9%, 82.9, 400 cycles, 1C, 55 °C
5 wt% Al_2O_3 [33]	76.1%, 90.2, 25 cycles, 0.2C, 55 °C
2 wt% Li_2MnO_3 [34]	89.5%, 108.2, 100 cycles, 0.2C, 55 °C
3 wt% TiO_2 [35]	77.1%, 97.5, 250 cycles, 1C, 55 °C
3 wt% $Co_3(PO_4)_2$ [36]	88.0%, 112.8, 100 cycles, 1C, 60 °C
3 wt% AlP [37]	87.0%, 108.7, 100 cycles, 1C, 60 °C
2 wt% $LaPO_4$ [38]	84.0%, 86.5, 100 cycles, 0.5C, 60 °C
Two step coating 1.5 wt% Al_2O_3 (this work)	86.8%, 92.5, 300 cycles, 1C, 60 °C

Cycling performance for the three different $LiMn_2O_4$ samples was measured at elevated temperature (60 °C) and a current density of 1 C between 3.0 - 4.3 V. As shown in Figure. 5, the specific discharge capacity of the pristine $LiMn_2O_4$ fades from 108.1 mAh g^{-1} to 46.6 mAh/ g^{-1} after 300 cycles, with a capacity retention rate of 43.1%. In comparation, for the Al_2O_3-coating sample, the cycling performances are all improved. The discharge capacity $LiMn_2O_4$/Al_2O_3 fades from 107.2 mAh g^{-1} to 71.5mAh/ g^{-1}, with a capacity retention rate of 66.7%, which is supported by our previous studies [25]. As for the two-step coating sample, $LiMn_2O_4$ /Al_2O_3-T exhibits almost the same initial discharge capacity of 106.6 mAh g^{-1} with the pristine sample, after 300 cycles, the discharge capacity maintains 92.5 mAh g^{-1}, with a capacity loss of only 86.8%. This indicates that the cyclic stability of $LiMn_2O_4$ at 60 °C is further significantly improved after two step coating. Furthermore, the electrochemical performance of our $LiMn_2O_4$ /Al_2O_3-T electrode was compared with that of other recently related reported in the literature (Table 1). Compared with these reports, one of the advantages of the method

in this paper is the $LiMn_2O_4$ /Al_2O_3-T electrode exhibits good capcity retentions (86.5%) after long circulation (300 cycles) at 60 °C. Therefore two step coating Al_2O_3 can effectively avoid electrolyte etching at elevated temperature, such outstanding cycling stability is not only better than that of pristine $LiMn_2O_4$, but also superior to the reported one step coating samples.

Figure. 6 shows the rate performance diagram of samples of pristine $LiMn_2O_4$, $LiMn_2O_4$ /Al_2O_3 and $LiMn_2O_4$/Al_2O_3-T at different charge and discharge currents. Among the samples, sample $LiMn_2O_4$/Al_2O_3-T had the best rate properties, at discharge currents of 0.2, 0.5, 1, 3, 5 and 10 C, the specific discharge capacity of the material was 114.2, 108.1, 105.3, 101.9 and 89.3 mAh g^{-1}, respectively. When the discharge current is reduced to 1 C, the specific discharge capacity of the material changes to 103.2 mAh g^{-1} after 50 cycles. Thus indicating the obvious amelioration of the capacity loss in the cycle after modification, two-steps coating can facilitate forming more compact ion conductive membrane, which can significantly improve the rate performance and cycling life of spinel $LiMn_2O_4$ [39, 40].

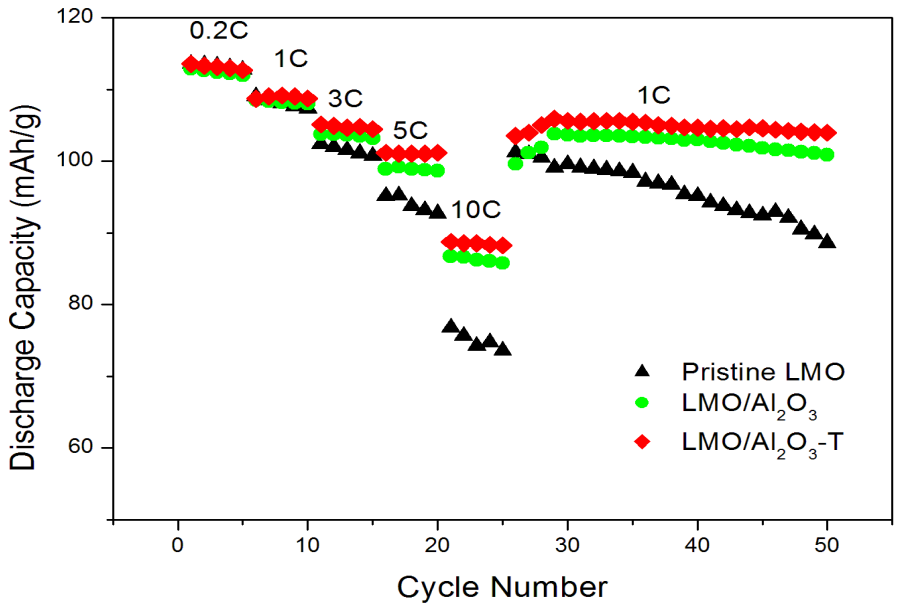

Figure 6. Cycling performance of the pristine $LiMn_2O_4$, $LiMn_2O_4$ /Al_2O_3 and $LiMn_2O_4$/Al_2O_3-T at 60 °C and different charge and discharge rate

The chemical composition of as-prepared samples were also determined by inductive coupled plasma emission spectrometer (ICP) and listed in Table 1. Although the expected coating amount is about only 1.5%, the actual Al_2O_3 quality percentage in $LiMn_2O_4$ /Al_2O_3 and $LiMn_2O_4$/Al_2O_3-T are almost equal, which are 1.491% and 1.488% respectively. Fig. 7 shows the manganese ion dissolution from the three spinel samples stored for 1, 2 and 3 weeks at 60 °C. After 1 week, the manganese ion dissolution for pristine $LiMn_2O_4$, $LiMn_2O_4$ /Al_2O_3 and $LiMn_2O_4$/Al_2O_3-T are 18, 32.5 and 60.8 ppm. The manganese ion dissolution for all of the three samples increase with increasing the storage time. After 3 weeks, the manganese ion dissolution for pristine $LiMn_2O_4$ is about 321.5 ppm, which is much more than that of the 1or 2 weeks ago. On the other hand, the manganese ion dissolution for $LiMn_2O_4$/Al_2O_3-T after 3 weeks is about 125.2 ppm, furthermore, the manganese ion dissolution for

$LiMn_2O_4/Al_2O_3$-T is reduced to 49.3 ppm, which is much less than that of the $LiMn_2O_4$ /Al_2O_3, although they have almost the same coating quantity. It is similar with the result reported by Yoshio et al. in the case of Al doped spinel [26]. This indicates that: (1) nano-Al_2O_3 coating can protect the spinel particles from negative electrolyte corrosion, (2) the two-step coating can further avoid the manganese ion dissolution in the electrolyte at high temperature [41,42].

Table 1. The Al_2O_3 content in the pristine $LiMn_2O_4$, $LiMn_2O_4$ /Al_2O_3 and $LiMn_2O_4/Al_2O_3$-T.

Sample name	Al_2O_3 content	Synthetic method
$LiMn_2O_4$	0.000%	Solid-state method
$LiMn_2O_4$ /Al_2O_3	1.491%	One-step coating method
$LiMn_2O_4/Al_2O_3$-T	1.488%	Two-step coating method

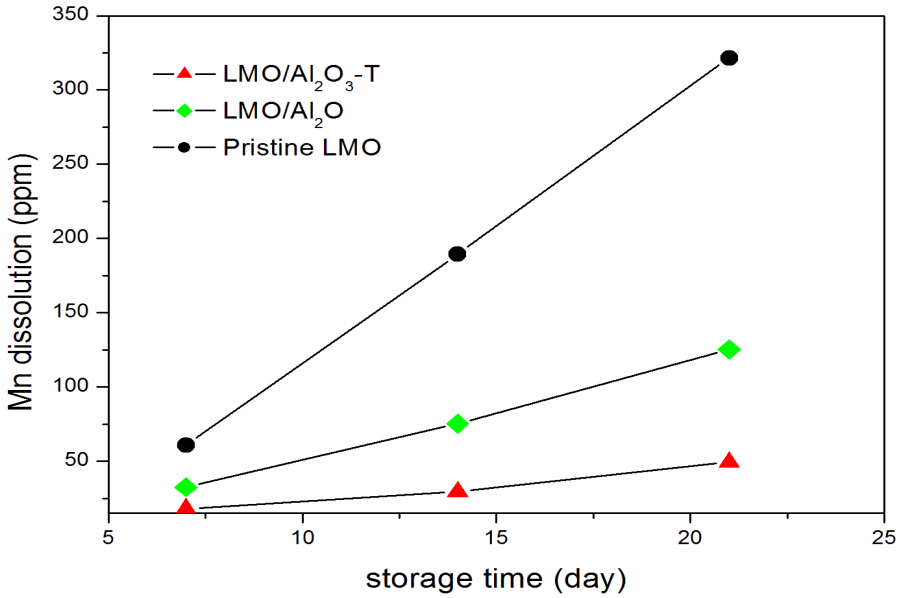

Figure 7. The relation of storage time and the manganese ion dissolution in electrolyte for different samples at 60 °C.

4. CONCLUSION

Within this work, nano- Al_2O_3 coating layers on spinel $LiMn_2O_4$ have been introduced by using a simple two step coating method. Compared with the samples of pristine and one step coating, the new samples exhibit more compact and uniform coating layers with the significantly enhanced cycling and rate performance at 60 °C, especially it exhibits capcity retentions of nearly 90% after 300 cycles at the elevated temperature. In addition, the manganese ion dissolution under the same condition is also effectively suppressed by two step coating. The surface coating quality is believed to be an important factor affecting the interfacial reaction behavior and electric performance of spinel, although they has the equal coating amount.

ACKNOWLEDGEMENT
The project was supported by National Natural Science Foundation of China (No.51604132) (No.51601081).

References

1. J. B. Goodenough and K. S. Park, *Journal of the American Chemical Society*., 135 (2013) 1167.
2. Dunn. B, H. Kamath and J. M. Tarascon, *Science*., 334 (2011) 928.
3. Q. Zhang and X. Li, *Int. J. Electrochem. Sci*., 8 (2013) 6449.
4. X. Hao , X. Lin, W. Lu and B. M. Bartlett, *Acs Applied Materials & Interfaces.*, 6 (2014) 10849.
5. D. Luo, G. Li, C. Fu, J. Zheng, J. Fan, Q. Li, *Advanced Energy Materials*., 4 (2014) 1220.
6. K. M. Shaju and P. G. Bruce, *Chemistry of Materials*., 20 (2008) 5557.
7. O. K. Park, Y. Cho, S. Lee, H. C. Yoo, H. K. Song and J. Cho, Energy & *Environmental Science*., 4 (2011) 1621.
8. K. M. Shaju and P. G. Bruce, *Chemistry of Materials*., 20 (2008) 5557.
9. M. J. Lee, S. Lee, P. Oh, Y. Kim and J. Cho, *Nano Letters*., 14 (2014) 993.
10. W. Tang, Y. Hou, F. Wang, L. Liu, Y. Wu and K, Zhu, *Nano Letters*., 13 (2013) 2036.
11. X. M. Liu, Z. D. Huang, S. Oh, P. C. Ma, P. C. Chan, G. K. Vedam, K. Kang and J. K. Kim, *J. Power Sources*., 195 (2010) 4290.
12. C. Qing, Y. Bai, J. Yang and W. Zhang, *Electrochim. Acta*., 56 (2011) 6612.
13. C. Li, H. P. Zhang, L. J. Fu, H. Liu, Y. P. Wu, E. Rahm, R. Holze and H. Q. Wu, *Electrochim. Acta*., 51 (2006) 3872.
14. W. Tang, L.L. Liu, S. Tian, L. Li, L.L. Li, Y.B. Yue, Y. Bai, Y.P. Wu, K. Zhu, R. Holze, *Electrochem. Commun*., 13 (2011) 1159.
15. M. Zhao, X. Song, F. Wang, W. Dai and X. Lu, *Electrochim. Acta*., 56 (2011) 5673.
16. J. Tu, X. B. Zhao, J. Xie, G. S. Cao, D. G. Zhuang, T. J. Zhu and J. P. Tu, *Journal of Alloys & Compounds*, 432 (2007) 313.
17. S. T. Myung, K. Izumi, S. Komaba, Y. K. Sun, H.Yashiro and N. Kumagai, *Chem. Mater.*, 17 (2005) 3695.
18. L. Wang, J.Zhao, S. Guo, X. He, C. Jiang, C. Wan, *Int. J. Electrochem. Sci*., 5 (2010) 1113.
19. S. K. Hu, G. H. Cheng, M. Y. Cheng, B. J. Hwang, R. Santhanam, *Journal of Power Sources*., 188 (2009) 564.
20. J. Gnanaraj, V. Pol, A. Gedanken and D. Aurbach, *Electrochem. Commun*., 5(2003) 940.
21. Y. Fan, J. Wang, Z. Tang, W. He and J. Zhang, *Electrochim. Acta*., 52 (2007) 23870.
22. M.Y. Cho, Roh. K. C, S. M. Park, M. S and J. W. Lee, *Materials Letters*., 65 (2011) 2011.
23. L. Feng, S. Wang, L. Han, X. Qin, H. Wei and Y.Yang, *Materials Letters*., 78 (2012)116.
24. Y. Zhang, Y. Zhang, P. Dong, B. Xia and R. Yang, *Chinese Journal of Rare Metals*., 38 (2014) 1030.
25. Y. Xia, Q. Zhang, H. Wang, H. Nakamura, H. Noguchi, M. Yoshio, *Electrochim. Acta*., 52 (2007), 4708.
26. C. Guo, M. Wang, T. Chen, X. Lou and C. Li, *Advanced Energy Materials*., 1 (2011) 736.
27. J. S. Kim, K. S.Kim, W. Cho, W. H. Shin, R. Kanno and J. W. Choi, *Nano Letters*., 12 (2012) 6358.
28. H. Xia, K. R. Ragavendran, J. Xie and L. Lu, *Journal of Power Source*., 9 (2012) 28.
29. G. H. Waller, P. D. Brooke, B. H. Rainwater, S. Y. Lai, R. Hu, Y. Ding, F. M. Alamgir, K. H. Sandhage and M. L. Liu, *Journal of Power Sources*., 306 (2016) 162.
31. J. Zeng, M. Li, X. Li, C. Chen, D. Xion, L. Dong, D. Li, A. Lushington and X. Sun, *Applied Surface Science*., 317 (2014) 884.
32. T, Artur, Y. D. Park, and J. Mun. *Journal of Power Sources*., 325(2016) 360.
33. T. Qiu, J. Wang, Y. Lu, and W. Yang, *Electrochimica Acta*., 147(2014) 626.
34. W. K. Kim, D. W. Han, W. H. Ryu, S. J. Lim and H. S. Kwon, *Electrochimica Acta*., 3 (2012) 17.

35. C. Zhang, X. Liu, Q. Su, J. Wu, T. Huang and A. Yu, *Sustainable Chem. Eng*., 5 (2016) 640.

36. X. Feng, J. Zhang and L. Yin, *Powder Technology*., 287 (2016) 77.
37. X. Feng, J. Zhang and L. Yin, *Materials Research Bulletin*., 74 (2015) 421.
38. P. Mohan, and G. P. Kalaignan. *Ceramics International*., 40 (2014) 1415.
39. M. X. Liu, L. H. Gan, W. Xiong, Z. Xu, D. Zhu and L. Chen, *Journal of Materials Chemistry A*., 2 (2014) 2555.
40. F. Y. Cheng, H. B. Wang, Z. Q. Zhu, Y. Wang, T. R. Zhang, Z. L. Tao and J. Chen, *Energy Environ. Sci*., 4 (2011), 3668.
41. Y. Shi, S. L. Chou, J. Z. Wang, D.Wexler, H. J. Li, H. K. Liu and Y. Wu, *Journal of Materials Chemistry*., 22 (2012) 16465.
42. H. K. Noh, H. S. Park, H. Y. Jeong, S. U. Lee, and H. K. Song, *Angewandte Chemie*., 126 (2014) 5059.